PCCP

Accepted Manuscript

ROYAL SOCIETY OF CHEMISTRY

www.rsc.org/pccp

A class of rare antiferromagnetic metallic oxides: Double perovskite $AMn_3V_4O_{12}$ (A = Na^+, Ca^{2+}, and La^{3+}) and the site-selective doping effect

Guangbiao Zhang,[a] Yuanxu Wang,*[a] Zhenxiang Cheng,*[a,b] Yuli Yan,[a] Chengxiao Peng,[a] Chao Wang,[a] and Shuai Dong[c]

Received Xth XXXXXXXXXX 20XX, Accepted Xth XXXXXXXXX 20XX
First published on the web Xth XXXXXXXXXX 200X
DOI: 10.1039/b000000x

We have investigated the structural, electronic, and magnetic properties of A-site-ordered double-perovskite-structured oxides, $AA'_3B_4O_{12}$ (A = Na, Ca, and La) with Mn and V at A′ and B sites, respectively, using first-principle calculations based on the density functional theory. Our calculation results show that the antiferromagnetic phase is the ground state for all the compounds. By changing the A-site ions from Na^+ to Ca^{2+} and then to La^{3+}, the transfer of charge between Mn and O ions was changed from 1.56 to 1.55 and then to 1.50, and that between the V and O ions changed from 2.01 to 1.95 and then to 1.93, revealing the cause for the unusual site-selective doping effect. Mn 3d electrons dominate the magnetic moment and are localized, with an intense hybridization with O 2p orbitals, which indicates that the magnetic exchange interaction between Mn ions is mediated through O and that the super exchange mechanism will take effect. These materials have a large one-electron bandwidth W, and the ratio of the on-site Coulomb repulsion U to W is less than a critical value $(U/W)_c$, which leads to metallic behavior of the $AMn_3V_4O_{12}$. This is further evidenced by the large number of free electrons contributed by V at the Fermi surface. These calculations, in combination with the reported experimental data, prove that these double perovskites belong to the rare antiferromagnetic metallic oxides.

1 Introduction

The A-site-ordered double perovskites with the general chemical formula $AA'_3B_4O_{12}$ (in which the B sites can sometimes accommodate two different elements) have received extensive attention both in theory and in experiments, due to their special ordered structures and wide variety of intriguing physical properties[1–5]. For instance, colossal magnetoresistance under weak magnetic fields, giant dielectric constants over a wide temperature range, and high temperature ferromagnetic (FM) transitions have all been found in such perovskites. Furthermore, the double perovskite structures provide an excellent platform that allow us to delicately tune its physical properties by accommodating substitution atoms on many sites, A, A′, and B. These compounds crystallize in an $Im\bar{3}$ cubic lattice, in which the A- and A′-site cations are at the originally 12-fold-coordinated site in a simple ABO_3 perovskite. The BO octahedron in this structure is fairly rigid but heavily tilted. The B-O-B angle deviates significantly away from 180°, leading to the formation of square planar-coordinated $A'O_4$ units. The A′ sites are usually filled with transition-metal Jahn-Teller-active ions such as Cu^{2+} and Mn^{3+}. For example, $ACuM_3Mn_4O_{12}$ (A = Ca, La, or Bi) compounds were observed to pass through a high-temperature ferromagnetic transition due to the coupling between the spins at A′-site Cu and B-site Mn above room temperature[6–8]. $LaCu_3Fe_4O_{12}$ and $BiCu_3Fe_4O_{12}$ show intersite charge transfer between the A-site Cu and the B-site Fe ions, wich leads to paramagnetism-to-antiferromagnetism (PM to AFM) transition, accompanied by a metal-to-insulator (semiconductor) isostructural phase transition[9,10]. In $CaCu_3B_4O_{12}$[11], In CuO_4 planes with Jahn-Teller Cu^{2+} ions are align perpendicularly to each other. This special alignment enables direct exchange interaction between the nearest Cu^{2+} spins, which gives rise to ferromagnetic behavior in $CaCu_3Ge_4O_{12}$ and $CaCu_3Sn_4O_{12}$. Whereas in $CaCu_3Ti_4O_{12}$, a superexchange interaction exists due to the Cu(3d)-O(2p)-Ti(3d) orbital hybridization, resulting in an antiferromagnetic insulating state, which makes the observation of its colossal dielectric constant possible. In $YMn_3Al_4O_{12}$[4], the half-filled d_{r2-z2} and d_{xy} orbitals of the nearest neighbor Mn ions are directed towards each other. The overlap of these

0[a] *Institute for Computational Materials Science, School of Physics and Electronics, Henan University, Kaifeng, 475004, People's Republic of China. E-mail: wangyx@henu.edu.cn*
0[b] *Institute for Superconducting & Electronic Materials (ISEM), University of Wollongong, North Wollongong NSW 2500, Australia. E-mail: cheng@uow.edu.au*
0[c] *Department of Physics, Southeast University, Nanjing, 211189, People's Republic of China*

orbitals produces an antiferromagnetic direct exchange interaction between the Mn spins. Therefore, it is quite obvious that charge transfer and orbit hybridization in $AA'_3B_4O_{12}$ compounds are critical for showing rich physics ranging from metal/insulator and ferromagnetism/antiferromagnetism transitions to the colossal magnetic resistance effect, and to giant dielectric constants. Understanding the mechanisms behind of this rich physics will help in the rational development of materials with superior properties.

Furthermore, antiferromagnetic metallic perovskite oxides are very rare. The transition-metal oxides belong to two categories, viz. the Mott-Hubbard type and the charge-transfer type[12]. The basis for such a classification depends on the relative value of the on-site Coulomb repulsion (U) between the d electrons and the one-electron bandwidth (W)[13]. In the limit of large U, the system is a Mott-Hubbard insulator, and the 3d orbitals are singly occupied sites. Such a system can be described by the antiferromagnetic Heisenberg spin model. On the other hand, in the opposite limit of large W, a system of uncorrelated half-filled bands becomes a nonmagnetic metal. Some perovskite transition-metal oxides, however, show a strong hybridization between the metal 3d and O 2p orbitals. This leads to an intermediate value of U/W, and the system has an antiferromagnetic metal ground state. The critical value $(U/W)_c$ is about 3[13]. Examples include $CaCrO_3$[13], $(La_{1-z}Nd_z)_{1-x}Sr_xMnO_3$[14], $Pr_{0.5}Sr_{0.5}MnO_3$[15], etc., where the system has an antiferromagnetic metal ground state. Although these materials are very useful for novel antiferromagnetic spintronic devices, they are very rare.

Very recently, site-ordered double perovskite $AMn_3V_4O_{12}$ (A = Na, Ca, La) compounds were synthesized using a high-pressure, high-temperature method by Zhang et al.[16] It has been shown experimentally that such a system has an antiferromagnetic/spin-glass-metallic ground state, accompanied by metallic behavior. In this study, we propose that the structure of such a perovskite structured system with two alternatives can be tuned, in contrast to simple perovskite, as a platform for rare antiferromagnetic metallic oxides, and their mechanism can be studied using first-principles density functional theory (DFT).

2 Computational Details

In this work, the structure optimization was carried out in the Kohn-Sham framework using the Vienna *ab initio* simulation package (VASP)[17–20], based on the projector-augmented-wave method[21,22]. The exchange-correlation energy was treated in the local spin-density approximation (LSDA)[23]. Actually, we also did the calculations based on the generalized gradient approximation (GGA), although, our results show that our Local density approximation (LDA) result is in accordance with experimental work, while the GGA results are not. For example, experimental work has shown that $CaMn_3V_4O_{12}$ is antiferromagnetic, and LDA shows the same. The GGA results, however, indicate that the FM structure is more favored in energy over the AFM by 37 meV. The present calculations do not include spin-orbit corrections. The Na ($2p^63s^1$), Ca ($2p^63s^2$), La ($5s^25p^65d^16s^2$), Mn ($3p^63d^54s^2$), V ($3p^63d^44s^1$), and O ($2s^22p^4$) electrons were treated as valence electrons. The plane wave cut-off energy was chosen to be 500 eV. The k-points of a 7×7×7 grid were generated using the Monkhorst-Pack scheme[24] in the Brillouin zone. Brillion zone integrations were performed with a Gaussian broadening[25] of 0.2 eV during all relaxations. Structural optimizations with the conjugate-gradient algorithm were continued until the Hellmann-Feynman forces on each ion to were less than 5 meV/Å. Experimentally established structural data[16] were used as input for the calculations.

In the LSDA+U framework[26,27], the strong Coulomb repulsion between localized d states is treated by adding a Hubbard-like term to the effective potential, leading to an improved description of the correlation effects in transition-metal oxides. Since there is no unique way of including a Hubbard term within the DFT framework, several different approaches exist, which all give similar results. To investigate the electron correlation effect on Mn and V 3d orbitals, we use the approach described by Dudarev et al.[28], where only an effective Hubbard parameter $U_{eff} = U - J$ enters the Hamiltonian, where U and J are the Coulomb and exchange parameters, respectively. We applied the values U_{Mn}=2, 4 eV and U_V= 2 eV. With these values of the Hubbard parameter, the calculated magnetic moment agree with the experimental data[16]. The experimental data show that valence states of V are 4+ and 3.75+. The number of 3d electrons of V is 1 and 1.25, and the number of 3d electrons determines the magnetic moment. When U = 2 eV is used for V, the calculated magnetic moment is 0.99 μB, 1.20 μB, and 1.40 μB for $NaMn_3V_4O_{12}$ (NMVO), $CaMn_3V_4O_{12}$ (CMVO), and $LaMn_3V_4O_{12}$ (LMVO), respectively. Therefore we think that U = 2 eV is the proper parameter for V, which well reflects the real situation. For the Mn case, the valence states are 2.33+ and 2+. The number of 3d electrons of Mn is 4.67 and 5. When U = 2 eV is used for Mn, the calculated magnetic moment is 3.9 μB, 3.96 μB, and 4.0 μB. When U = 4 eV, the calculated magnetic moment is 4.14 μB, 4.21 μB, and 4.24 μB. Therefore, we think that U = 4 eV is the proper parameter for Mn, which well reflects the real situation.

3 Results and Discussion

$AMn_3V_4O_{12}$ (AMVO) is a cubic A-site-ordered family of compounds in the space group $Im\bar{3}$ (No. 204)[16], in which the A, Mn, V, and O atoms are placed at the 2*a* (0, 0, 0), 6*b* (0, 1/2, 1/2), 8*c* (1/4, 1/4, 1/4), and 24*g* (x, y, 0) positions, respectively (shown in Figure 1 a). Experimentally established structural

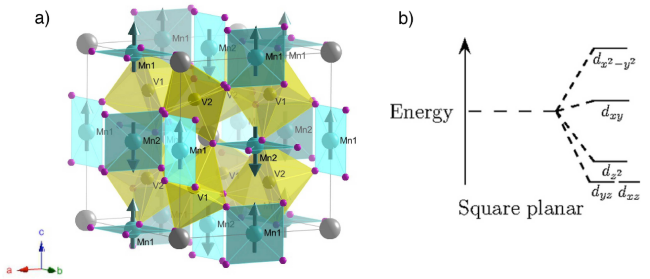

Fig. 1 a) Crystal structure of the A-site-ordered pervoskites $AMn_3V_4O_{12}$ in space group $Im\bar{3}$. The arrows indicate the spin direction. b) Mn atom 3d sub-orbital diagram in compounds.

data were used as input for the calculations. The optimized structural parameters and selected bond lengths and angles of the AMVO compounds are listed in Table 1 along with experimental results for comparison. Both the theory and the experimental results show that the lattice parameter, the Mn-Mn distance, the Mn-O distance, and the V-O distance will increase when the A-site ions change from Na to Ca and then to La due to the increased atomic size. The optimized structural parameters are smaller than the experimental ones. The underestimation of structural parameters for LDA comes from the overbinding effect [29].

We calculated the total energy with respect to the ground state magnetic configuration of $AMn_3V_4O_{12}$ using the LSDA method. To explore the structural phase stability of AMVO, we considered G-type antiferromagnetic (G-AFM), A-type antiferromagnetic (A-AFM), and ferromagnetic (FM) orderings. We found the G-AFM phase to be the ground state for NMVO. For NMVO, it is 47 meV/f.u. lower in energy than the A-AFM state and 35 meV/f.u. lower than the FM state. For CMVO, it is 10 meV/f.u. lower than the A-AFM state and 19 meV/f.u. lower than the FM state. For LMVO, it is 20 meV/f.u. lower than the A-AFM state and 66 meV/f.u. lower than the FM state.

Table 1 Structural parameters and selected bond lengths and angles of NMVO, CMVO, and LMVO optimized by VASP, including the experimental (Exp.) structural parameters [16] as a reference.

	NMVO		CMVO		LMVO	
	Theo.	Exp.	Theo.	Exp.	Theo.	Exp.
a(Å)	7.2072	7.35514	7.2363	7.40704	7.30489	7.48485
O_x	0.3074	0.3023	0.3038	0.2944	0.3047	0.2947
O_y	0.1856	0.1917	0.1833	0.1936	0.1829	0.1957
Mn-O(Å)	1.928×4	2.032×4	1.943×4	2.092×4	1.955×4	2.124×4
	2.658×4	2.695×4	2.696×4	2.733×4	2.721×4	2.753×4
	3.169×4	3.169×4	3.176×4	3.147×4	3.213×4	3.170×4
V-O(Å)	1.906×6	1.925×6	1.908×6	1.927×6	1.926×6	1.944×6
V-O-V(deg)	141.9	145.6	142.2	147.98	141.8	148.6
Mn-O-Mn(deg)	102.4	101.4	101.3	99.4	101.5	99.6

Considering the electron correlation in the 3d transition-metal Mn and V ions, we calculated the electronic and magnetic properties of AMVO using the LSDA and LSDA+U methods. The effective Hubbard parameter of Mn is 0 (LSDA), 2, and 4 eV and that of V is 0 (LSDA) and 2 eV. Figure 2 presents the total and site-decomposed density of states (DOS) in the AFM configuration for AMVO. In agreement with the experimental results, it was found that the three compounds are metallic, as evidenced by the large number of states around the Fermi surface. Therefore, these compounds belong to a very rare class of materials, metallic antiferromagnetic perovskite oxides. Although the bands at the Fermi surface are mainly composed of bands from V, a very small proportion of contribution from O and Mn is also observed, which indicates a certain degree of orbital hybridization among the orbitals of these ions. For NMVO, the bands (at about -2 eV), which are composed of Mn 3d and O 2p orbitals, suggest that there is considerable Mn-O covalent hybridization, which indicates a superexchange mechanism for the antiferromagnetism. The Mn-O squares, however, do not share oxygen atoms, but instead, they form O-Mn-O-O-Mn paths. The Mn-O-Mn superexchange interaction does not seem to be responsible for the antiferromagnetism of AMVO because one of the Mn-O bond lengths (greater than 2.6 Å) in the Mn-O-Mn paths is too long to mediate such an interaction and because the Mn-O-Mn bond angle (about 103°) is far from the 180° expected to induce antiferromagnetic interaction according to the Kanamori-Goodenough rule [30–32]. The orbital hybridization of V, O, and Mn orbitals at the Fermi surface indicates that the B-site V ions may mediate the antiferromagnetic interaction between the Mn spins through Mn-O-V-O-Mn paths. This may be the origin of the antiferromagnetism in such metallic systems [4].

The LSDA+U results retain this metallic character. The band gap between the conductantion bands and valence bands is enlarged due to orbital shifting towards higher energy with as the U value increases. The band gap increases from 0.8 to 1.1 and then to 1.2 eV with U_{Mn} increasing from 0 to 4 eV and U_V increasing from 0 to 2 eV. Meanwhile, the calculated magnetic moment at the Mn-site changes from 3.70 to 4.14 μ_B, from 3.75 to 4.21 μ_B, and from 3.76 to 4.24 μ_B with U_{Mn} increasing from 0 to 4 eV for NMVO, CMVO, and LMVO, respectively. The calculated magnetic moment at the V-site, however, changes from 0.01 to 0.99 μ_B, from 0.35 to 1.20 μ_B, and from 0.78 to 1.41 μ_B as U_V increases from 0 to 2 eV for NMVO, CMVO, and LMVO, respectively. The qualitative change indicates that the electronic repulsion of the V 3d electron is very much correlated within AMVO.

The partial density of states (PDOS) curves of Mn1 in the three compounds, NMVO, CMVO, and LMVO, are shown in Figure 3, respectively. The doped electrons of the A′-site Mn ions are mainly localized below the Fermi surface, in addition to a very small proportion of electrons at the Fermi surface,

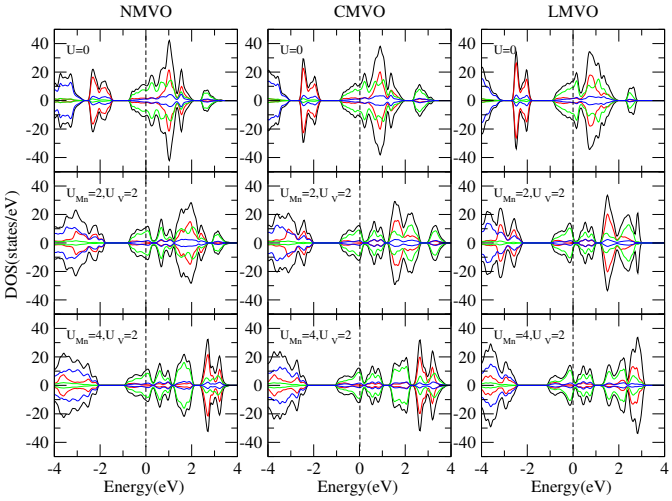

Fig. 2 The total and site-decomposed electronic DOS for the AFM configuration of NMVO, CMVO, and LMVO obtained by LSDA and LDA+U calculations: total DOS (black), Mn (red), V (green), O (blue). The vertical dashed line at zero indicates the Fermi energy level.

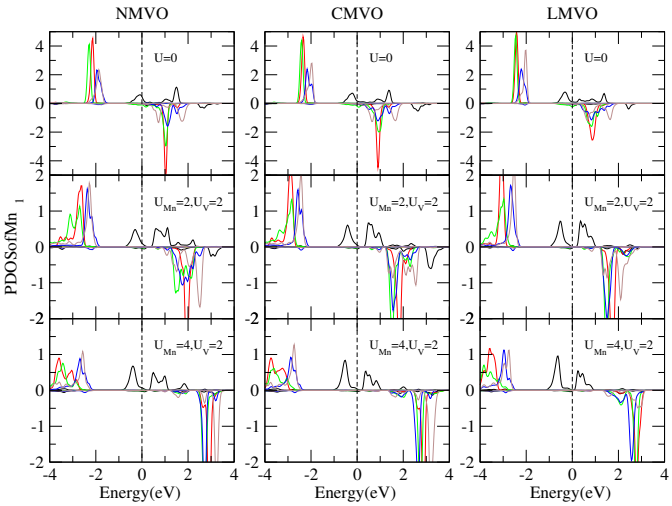

Fig. 3 The PDOS of Mn for the AFM configuration of a) NMVO, b) CMVO, and c) LMVO obtained by LDA and LDA+U calculations: d_{xy} (black), d_{yz} (red), d_{xz} (green), d_{z^2} (blue), d_x^2 (brown). The vertical dashed line at zero indicates the Fermi energy level.

which means that the Mn ions are responsible for the magnetic moment in the compounds. On the other hand, the electrons of B-site V ions are mainly located at the Femi surface, which means that they are delocalized and contribute to the conductivity. According to the PDOS, the energy level diagrams of A′-site Mn 3d orbitals in the three compounds have been plotted and are shown as Figure 1b. The Mn $3d_{yz}$, $3d_{xz}$, $3d_{x^2}$, and $3d_{y^2}$ sub-orbitals are fully occupied by electrons and located around 2 eV below the Fermi level, while the $3d_{xy}$ ones are located at the Fermi surface with partial occupation of electrons. This indicates that Mn $3d_{xy}$ electrons partially contribute to the conductivity of the compounds in addition to the contribution to the magnetic moment. This indicates that the Mn is in the high spin states in all three compounds. The calculated magnetic moments are smaller than the expected magnetic moment value of 5 μ_B[33]. Due to the partial occupation of the $3d_{xy}$ orbital and the considerable Mn-O covalent hybridization, a small magnetic moment exists at the oxygen sites. These values are 0.04, 0.04, and 0.03 μ_B for NMVO, CMVO, and LMVO, respectively. This further proves that the Mn 3d, O 2p, and V 3d orbital hybridization is the key to the antiferromagnetic ordering in these compounds.

The V-O distances are 1.906, 1.908, and 1.926 Åfor NMVO, CMVO, and LMVO, respectively. These values are similar to the average values of the V-O distance n metallic perovskite-type V oxides for $SrVO_3$ (1.921 Å)[34], $MnVO_3$ (1.938 Å)[33], and $CaVO_3$ (1.963 Å)[35], and are less than the average values of the V-O distance in insulator perovskite-type V oxides for $ScVO_3$ (2.003Å)[36], YVO_3 (2.007 Å)[37], and $LaVO_3$ (2.042 Å)[37]. The short V-O distance implies the strong hybridization of the V 3d and O 2p orbitals, and it leads to a large one-electron bandwidth W. For the intermediate values of U/W, the materials are metals.

We also used Bader's "atoms in molecules" theory[38,39] to analyze the valence states of the Mn and V ions. Our calculations found that the transfer of charge between Mn and O ions changed from 1.56 to 1.55 and then to 1.50, and the transfer of charge between V and O ions changed from 2.01 to 1.95 and then to 1.93 on changing the A-site ions from Na^+ to Ca^{2+} and then to La^{3+}. These results are consistent with the observed results of the different charge densities, supporting the site-selective doping effect in these compounds.

4 Conclusions

In summary, based on first-principle calculations, we have studied the structural, electronic, and magnetic properties of A-site-ordered perovskite-structured oxides with Mn and V at the A and B sites, respectively. The total energy calculations reveal that the AFM phase has a lower energy than the FM phase. By changing the A-site ions from Na to Ca and from Ca to La, the transfer of charge between Mn and O ions changed from 1.56

to 1.55 and then to 1.50, and the transfer of charge between V and O ions changed from 2.01 to 1.95 and then to 1.93. The hybridization of the A-site Mn 3d and O 2p orbitals below the Fermi surface dominates the magnetic moment. The values of the V-O distances are similar to the average values of the V-O distance for metallic perovskite-type V oxides. The short V-O distance implies a large one-electron bandwidth W. When the U/W ratio is less than a critical value $(U/W)_c$, the materials are metallic. In the mechanism for such unique metallic antiferromagnetic behavior in double perovskite oxides, Mn contributes magnetic moment, while V contributes the metallic behavior, which is different from that in previously reported compounds, such as $CaCrO_3$, where Cr contributes both the magnetic moment and the free electrons at the Fermi level. This understanding opens up a new route to rational design of antiferromagnetic metallic oxides that will have applications in novel spintronics devices. In addition, the flexible structure with both the A(A′) and B sites modifiable provides an excellent playground for tuning properties by accommodating variable elements.

5 Acknowledgments

This research was sponsored by the National Natural Science Foundation of China (No. 21071045, U1204112, and 11305046), the Program for New Century Excellent Talents in University (No. NCET-10-0132), and Foundation of He'nan Educational Committee (No. 14B140003, 13A140076, 14A430029, and 14A140016). Z. X. Cheng thanks ARC for support through a Future Fellowship.

References

1 M. Imada, A. Fujimori and Y. Tokura, *Rev. Mod. Phys.*, 1998, **70**, 1039–1263.

2 E. Dagotto, T. Hotta and A. Moreo, *Physics Reports*, 2001, **344**, 1–153.

3 Y. Long, T. Saito, M. Mizumaki, A. Agui and Y. Shimakawa, *J. Am. Chem. Soc.*, 2009, **131**, 16244–16247.

4 T. Tohyama, T. Saito, M. Mizumaki, A. Agui and Y. Shimakawa, *Inorg. Chem.*, 2010, **49**, 2492–2495.

5 H. Li, S. Lv, Y. Bai, Y. Xia, X. Liu and J. Meng, *J. Comput. Chem.*, 2012, **33**, 82–87.

6 Z. Zeng, M. Greenblatt, M. A. Subramanian and M. Croft, *Phys. Rev. Lett.*, 1999, **82**, 3164–3167.

7 J. A. Alonso, J. Sánchez-Benítez, A. D. Andrés, M. J. Martínez-Lope, M. T. Casais and J. L. Martínez, *Applied Physics Letters*, 2003, **83**, 2623–2625.

8 K. Takata, I. Yamada, M. Azuma, M. Takano and Y. Shimakawa, *Phys. Rev. B*, 2007, **76**, 024429–.

9 Y. W. Long, N. Hayashi, T. Saito, M. Azuma, S. Muranaka and Y. Shimakawa, *Nature*, 2009, **458**, 60–U3.

10 Y. Long, T. Saito, T. Tohyama, K. Oka, M. Azuma and Y. Shimakawa, *Inorganic Chemistry*, 2009, **48**, 8489–8492.

11 H. Shiraki, T. Saito, T. Yamada, M. Tsujimoto, M. Azuma, H. Kurata, S. Isoda, M. Takano and Y. Shimakawa, *Phys. Rev. B*, 2007, **76**, 140403.

12 J. Zaanen, G. A. Sawatzky and J. W. Allen, *Phys. Rev. Lett.*, 1985, **55**, 418–421.

13 P. A. Bhobe, A. Chainani, M. Taguchi, R. Eguchi, M. Matsunami, T. Ohtsuki, K. Ishizaka, M. Okawa, M. Oura, Y. Senba, H. Ohashi, M. Isobe, Y. Ueda and S. Shin, *Phys. Rev. B*, 2011, **83**, 165132.

14 T. Akimoto, Y. Maruyama, Y. Moritomo, A. Nakamura, K. Hirota, K. Ohoyama and M. Ohashi, *Phys. Rev. B*, 1998, **57**, R5594–R5597.

15 R. Kajimoto, H. Yoshizawa, Y. Tomioka and Y. Tokura, *Phys. Rev. B*, 2002, **66**, 180402.

16 S. Zhang, T. Saito, M. Mizumaki, W.-t. Chen, T. Tohyama and Y. Shimakawa, *J. Am. Chem. Soc.*, 2013, **135**, 6056–6060.

17 G. Kresse and J. Hafner, *Phys. Rev. B*, 1993, **47**, 558–561.

18 G. Kresse and J. Hafner, *Phys. Rev. B*, 1994, **49**, 14251–14269.

19 G. Kresse and J. Furthmüller, *Computational Materials Science*, 1996, **6**, 15–50.

20 G. Kresse and D. Joubert, *Phys. Rev. B*, 1999, **59**, 1758–1775.

21 P. E. Blöchl, *Phys. Rev. B*, 1994, **50**, 17953–17979.

22 G. Kresse and D. Joubert, *Phys. Rev. B*, 1999, **59**, 1758–1775.

23 R. O. Jones and O. Gunnarsson, *Rev. Mod. Phys.*, 1989, **61**, 689–746.

24 H. Monkhorst and J. Pack, *Phys. Rev. B*, 1976, **13**, 5188–5192.

25 C. Elsässer, M. Fähnle, C. Chan and K. Ho, *Phys. Rev. B*, 1994, **49**, 13975–13978.

26 I. V. Solovyev, P. H. Dederichs and V. I. Anisimov, *Phys. Rev. B*, 1994, **50**, 16861–16871.

27 V. I. Anisimov, J. Zaanen and O. K. Andersen, *Phys. Rev. B*, 1991, **44**, 943–954.

28 S. Dudarev, G. Botton, S. Savrasov, C. Humphreys and A. Sutton, *Phys. Rev. B*, 1998, **57**, 1505–1509.

29 A. van de Walle and G. Ceder, *Phys. Rev. B*, 1999, **59**, 14992–15001.

30 J. B. Goodenough, *Phys. Rev.*, 1955, **100**, 564–573.

31 J. B. Goodenough, *Journal of Physics and Chemistry of Solids*, 1958, **6**, 287 – 297.

32 J. Kanamori, *Journal of Physics and Chemistry of Solids*, 1959, **10**, 87 – 98.

33 M. Markkula, A. M. Arevalo-Lopez, A. Kusmartseva, J. A. Rodgers, C. Ritter, H. Wu and J. P. Attfield, *Phys. Rev. B*, 2011, **84**, 094450.

34 Y. Lan, X. Chen and M. He, *Journal of Alloys and Compounds*, 2003, **354**, 95 – 98.

35 B. Chamberland and P. Danielson, *Journal of Solid State Chemistry*, 1971, **3**, 243 – 247.

36 G. Wang, J. Yang, C. Liu and M. Zhang, *Solid State Communications*, 2012, **152**, 2049–2052.

37 H. Sawada, N. Hamada, K. Terakura and T. Asada, *Phys. Rev. B*, 1996, **53**, 12742–12749.

38 R. F. W. Bader, in *Atoms in Molecules*, John Wiley & Sons, Ltd, 2002.

39 W. Tang, E. Sanville and G. Henkelman, *Journal of Physics-condensed Matter*, 2009, **21**, 084204.